AIAA SciTech Forum
11–15 & 19–21 January 2021, VIRTUAL EVENT
AIAA Scitech 2021 Forum

10.2514/6.2021-0937

Local Aero-Optical Measurements of a Wake behind a Cylinder in Turbulent Flow using a Focused Jitter Probe

Luke Butler[1], Stanislav Gordeyev[2]
University of Notre Dame, Notre Dame, IN, 46556

A novel point aero-optical measurement technique is presented, where a converging-diverging laser beam passing through a wind tunnel is used to perform localized aero-optical jitter measurements. Validating experiments were conducted using a subsonic speed tunnel. Measurements were performed in both an empty wind tunnel with only turbulent boundary layers present at the walls, and in the wake downstream of a small diameter cylinder placed in the middle of the test section to create local aero-optical distortions. Several measurements were conducted with the focal point placed at various spanwise locations across the flow. The analysis of the beam jitter spectra clearly demonstrates the ability of the focused jitter probe to measure aero-optical jitter primarily near the focal point, and to attenuate the jitter caused by the flow away from the focal point. In the case of the cylinder flow, when the focal point was placed inside the cylinder's wake, a weak spectral peak corresponding to the shedding frequency was clearly resolved despite the presence of the corrupting effects from the boundary layers at the walls of the tunnel. A traditional jitter probe, however, was unable to resolve this weak spectral peak. Various experimental and data processing requirements to obtain accurate spectra are also discussed. In future work, this technique will be expanded to incorporate two beams, referred to as a focused Malley probe, to perform local velocity measurements.

I. Introduction

As a laser beam passes through turbulent flow, aero-optical structures of fluctuating densities impose optical aberration on the beam and, among other things, will cause the beam to propagate in a different direction. This is known as beam deflection or beam jitter. For small beam diameters, Huygens principle states [1] that the beam will be deflected by an amount proportional to the 2-D gradient of optical path length (OPL),

$$\theta_x(t) = \frac{\partial}{\partial x} OPL(x,y,t),\ \theta_y(t) = \frac{\partial}{\partial y} OPL(x,y,t),$$

as schematically shown in Figure 1. OPL, in turn, is an integral of the density field along the beam propagation,

$$OPL(x,y,t) = K_{GD} \int \rho(x,y,z,t) dz,$$

where K_{GD} is Gladstone-Dale constant [1]. If the convective speed is known, OPL can be reconstructed from the deflection angle signals using the Taylor frozen field hypothesis [2,3],

[1] Graduate student, Department of Aerospace and Mech. Eng., AIAA Student member.
[2] Associate Professor, Department of Aerospace and Mech. Eng., AIAA Associate Fellow

$$OPL(t = -U_C x) = -U_C \int_{t_o}^{t} \theta(t)dt \ .$$

Thus, by projecting a single small-aperture laser beam through turbulent flows, wavefronts can be directly measured if the convective speed is known. As wavefronts are proportional to the integrated density field, analysis of the time series of deflection angles is very informative way to learn about the underlying turbulent flow. This approach was successfully used to study boundary layers [1,2,4], shear layers [1,5,6], and flows around turrets [3,7,8].

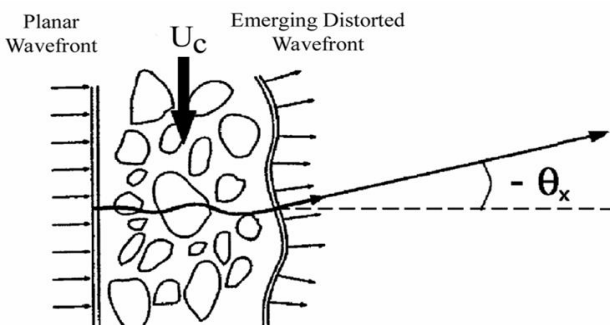

Figure 1: Beam deflection due to turbulent flow

The issue with this approach is that wavefronts are integrated quantities and do not provide any information about where along the laser beam the optical distortions happen. For spanwise-uniform flows, this problem can be addressed by collecting wavefronts in both wall-normal and spanwise directions [9], but it general it is a drawback of any optical technique involving a collimated laser beam.

While the source of beam jitter cannot be located along the beam, the amount of jitter depends on the beam aperture size. When the beam aperture is large compared to the aberrating optical structures, the contribution to the overall beam deflection is very small due to an aperture-averaging effect, which works as a low-pass filter, effectively suppressing high spatial frequencies present in the wavefronts [7,10]. Figure 2 presents the amount of beam jitter imposed on the laser beam by a turbulent subsonic boundary layer; the overall beam jitter for apertures larger than several boundary layer thicknesses is a hundred times less than for small-sized beams.

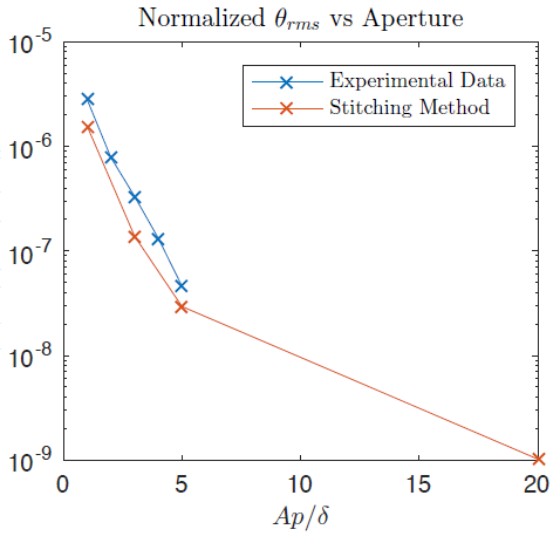

Figure 2: Normalized overall beam jitter due to a boundary layer as a function of the beam size, Ap. From [10].

Previous study has demonstrated the aperture low-pass filtering property, or aperture averaging effect, with constant-diameter laser beams of various apertures passing through the tunnel [11]. This study used a position sensing device, or PSD, to measure the global jitter for various beam sizes. The power spectra are shown in Figure 3 (Left). This plot demonstrates the effect of larger diameters acting as lower pass filters due to aperture averaging. The spikes at low frequency are due to mechanical vibration, the spikes at high frequency are due to electronic noise, and the leveling off at high frequencies is due to a noise floor. The data in Figure 3 (Right) is normalized on the y-axis to the local jitter and normalized on the x-axis to the aperture-dependent z-parameter, and compared with the theoretical model, or G-function.

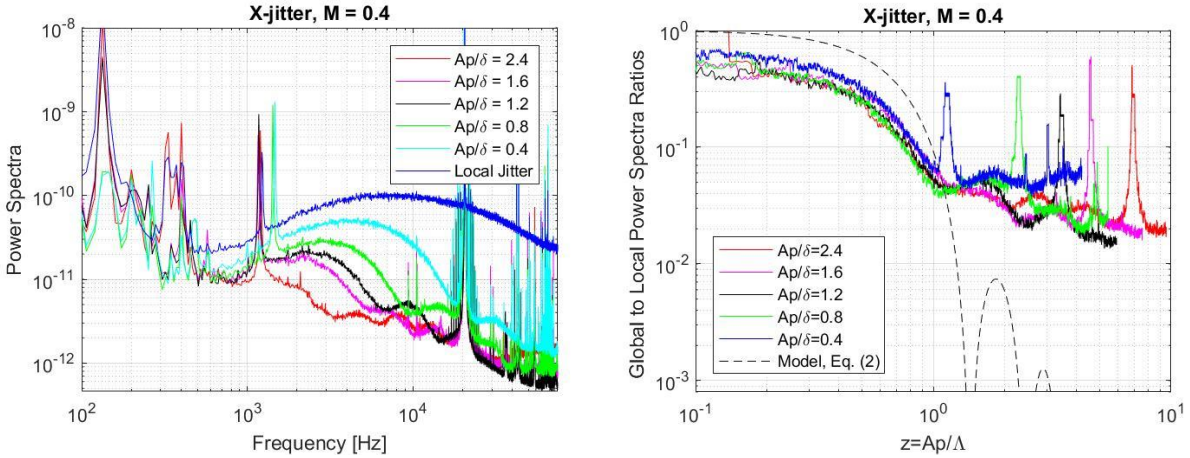

Figure 3: Power spectra of global beam jitter (Left) and ratios of global to local beam jitter power spectra (Right) for different beam apertures in the streamwise direction at a free stream Mach number of 0.4. From [11].

In [7] it has been shown that the theoretical ratio of global jitter spectral amplitude to local jitter spectral amplitude in the streamwise direction for one-dimensional periodic wavefront with a characteristic spatial wavelength, Λ, can be expressed through the aperture dependent transfer function, called $G(z)$,

$$G(z) = \frac{\theta_G(f;Ap)}{\theta(f)} = 2[sin(\pi z) - \pi z\, cos(\pi z)]/(\pi z)^3$$

where the parameter $z = {}^{Ap}/_{\Lambda}$ is the aperture diameter divided by the spatial wavelength. For convective structures traveling at the same speed of U_c, the spatial wavelength is defined as $\Lambda = U_c/f$, where of convective velocity U_c is approximately 0.82 of U_∞ for subsonic boundary layers [2].

The line-integral aero-optical measurement technique we are seeking to develop is a focused version of the Malley probe. The regular Malley probe consists of two parallel small-diameter laser beams passing through the tunnel with a small known separation distance in the streamwise direction [2,3]. The resulting jitter or deflection angles imposed on both beams are measured with position-sensing devices (PSDs) or a high-speed digital camera. By correlating the jitter time series, the time delay can be computed, and knowing the distance between the beams, the speed of the flow can be determined [2,3]. Henceforth, in order to differentiate from the two-beam Malley probe, the taking of jitter measurements from a singular beam shall be referred to as a jitter probe. This paper presents the results of a focused jitter probe, which future work will extend to the development and refinement of a focused Malley probe by adding a second jitter probe in such a way that two focal point measurements can be taken simultaneously a small distance apart.

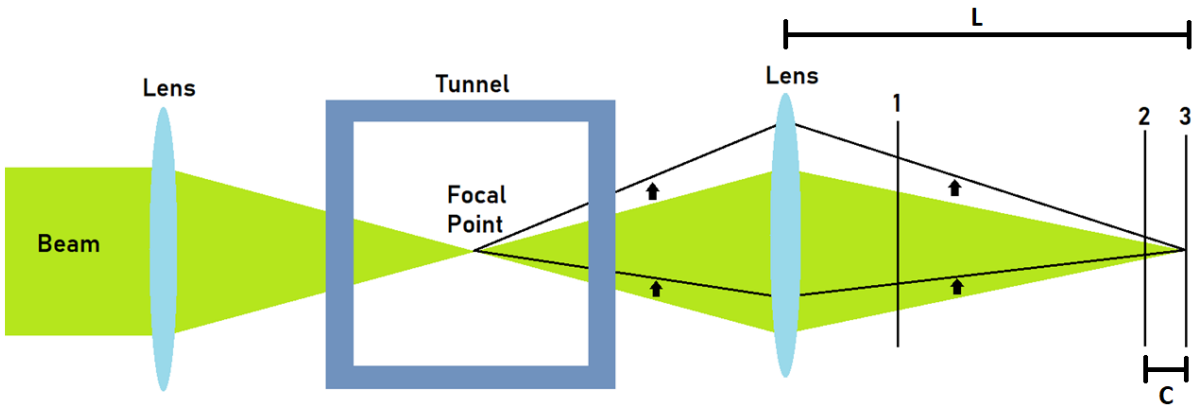

Figure 4: Conceptual schematics of convergent-divergent beam experiment

The general concept for a focused jitter probe is shown in Figure 4. A collimated beam with a large diameter is focused to a point inside the tunnel. After the focusing point, beam diverges and, after passing through a second focusing lens, is forwarded to a high-speed camera, or a position sensing device, to measure the overall global beam angular deflection. The total beam deflection is an integral of averaged-over-area beam deflections along the beam. Where the beam diameter is large compared to the aberrating optical structures, the contribution to the overall beam deflection is small due to the aperture-averaging effect. Consequently, boundary-layer-related optical effects on both sides of the tunnel windows, while typically large in amplitude, should not significantly contribute to the overall beam deflection. Only the focal point region, where the beam is small, has the largest effect on the total beam deflection. This means that the main contribution to the deflection of the beam occurs primarily along the portion of the beam near the focal point, where the beam has the smallest diameter. The deflection angles are given by the equations:

$$\theta_x(t) = \frac{\partial OPD(x,y,t)}{\partial x} \approx K_{GD} \frac{\partial}{\partial x} \int_{-l/2}^{l/2} \rho(x,y,z,t)dz = K_{GD} l \frac{\partial}{\partial x} \langle \rho(x,y,z,t) \rangle_l$$

$$\theta_y(t) \approx K_{GD} l \frac{\partial}{\partial y} \langle \rho(x,y,z,t) \rangle_l \quad ,$$

where l is the length of the beam with sufficiently small diameter and brackets denote along-the-beam averaging. Thus, the deflection angle or overall beam tilt is proportional to the density gradient near the focal point. The aperture-related analysis, provided in [7], assumed that wavefronts are one-dimensional and derived a transfer low-pass function relating small-aperture and large-aperture jitter spectra. As real wavefronts are two-dimensional, the transfer function will be different and depend on wavefront's spatial correlations in both dimensions. This effect has important implications in that it can be used for developing a new way of non-intrusively measuring density fluctuations near the region of the focal point. This measurement technique could be used in hypersonic tunnels, for instance, where the number of measurement techniques are limited due to the need for non-intrusive measurements and the lack of focused techniques that can discern weaker signals in the center of the tunnel from the strong boundary layer signals at the tunnel walls.

Another existing focused optical technique which looks similar, but uses a different mechanism to achieve a focusing effect, is known as focused laser differential interferometry, or FLDI [12-15]. Briefly, FLDI is a non-intrusive optical point measurement technique which measures the density gradient at the focus location. Because fluctuations in density alter the index of refraction and thus the speed of light through the medium, a density gradient between two nearby points will create different optical path lengths for light traveling through them. If beams that were originally in sync pass through these points, this difference in optical path length will create interference when the beams are recombined on the photodetector, with the variation in intensity proportional to this interference, the difference in optical path lengths, and the density gradient. This method works best when the differences are small enough that the linear approximation along a portion of the sine wave works well, but large enough that it overrides any electronic noise [12].

While FLDI offers an alternative focused optical technique for point optical measurements, the focused jitter probe and a proposed focused Malley probe could add additional focused point-measurement optical techniques to the toolbox. This paper presents the results of measurements with a focused jitter probe using this concept taken both in an empty tunnel and in the wake behind a spanwise-mounted cylinder in Mach 0.4 flow.

II. Experimental Set-Up

Experiments were performed using the 100x100 mm transonic in-draft wind tunnel at the Hessert Research Laboratory at the University of Notre Dame. The wind tunnel test section has optical quality glass installed on the sides where the laser beam was transmitted through. A variable intensity 532 nm YaG:Nd laser was expanded to 25.4 mm using a beam collimator. To demonstrate the feasibility of local measurements of the unsteady density field using a convergent-divergent beam, two lenses were placed at either end of the tunnel to have the light converged to a point at the center of the test section and converge toward a Phantom v1611 high speed camera after the test section, as shown in Figure 5(a). These lenses were attached to an apparatus allowing them to be translated in the spanwise z-direction in unison so the point could be moved to different spanwise locations in the test section. The camera was translated by the same distance. Depending on the setup, neutral density filters can be used to reduce the intensity of laser light going into the camera.

Looking back at Figure 4, it is important to note that due to reimaging, deflections at the focal point will result in zero deflection at position 3, so a sensor cannot be placed here to measure deflections. For this reason, in order to perform focused jitter measurements, the sensor must measure the beam displacement some distance away from the focal point, such as position 2, but not so far away that the beam would be so large that a high speed camera could not measure it at high frequency, such as would be the case with position 1. The distance the camera is placed away from the focal point C can be modified as a fraction of the total distance to the focusing lens, denoted as L in Figure 4.

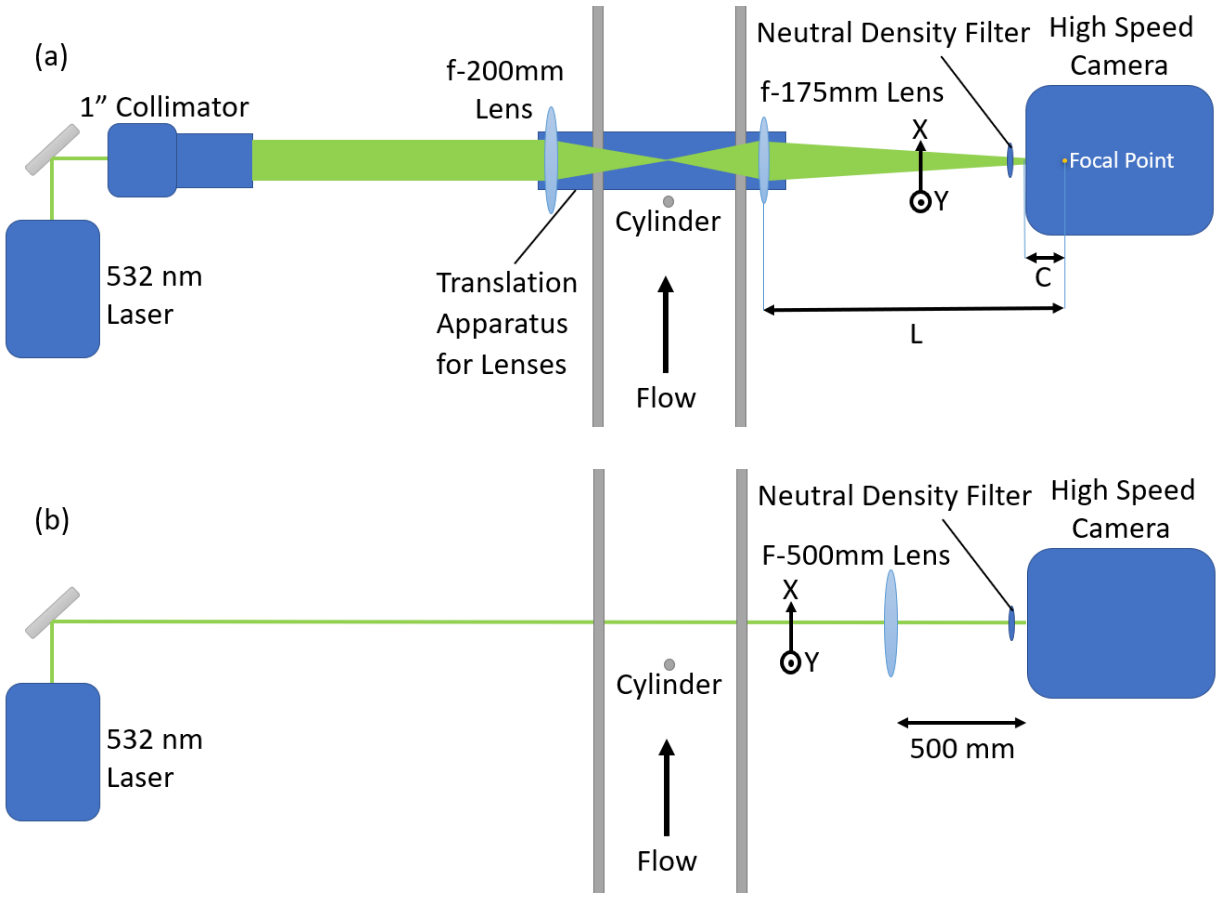

Figure 5 (a) Top-view schematic of experimental set-up for cylinder wake measurements with focused jitter probe. (b) Top-view schematic of experimental set-up for cylinder wake measurements with conventional jitter probe

Two sets of experiments were conducted at a Mach number of 0.4. The first one, labeled as the empty tunnel test, had turbulent boundary layers on the tunnel walls as the only source of aero-optical distortions. For the second experiment, additional localized optical distortions in the center of the tunnel were created by mounting a 3.175 mm diameter cylinder vertically in the test section. The cylinder formed a turbulent wake with vortex shedding at a theoretical frequency of $St_D = 0.2$ [16] or 9.55 kHz. In the second test, the sources of the beam jitter were the structures in the boundary layers and the structures in the wake of the cylinder. The purpose of the second test was to demonstrate that the focused jitter probe can measure aero-optical distortions due to only the cylinder's wake in the presence of the corrupting aero-optical distortions due to the boundary layers. Beam displacement measurements were taken with the focal point translated to various spanwise locations inside the tunnel, both with and without the cylinder present. With the cylinder present, the focal point was placed around 2 cm downstream of the cylinder. The camera was translated along with the apparatus to maintain the proper C/L ratio.

Although in order to maximize the attenuation achieved from aperture averaging, it is best to use the smallest possible focal length to achieve the largest possible diameter at the boundary layers, it was found during preliminary testing that lenses with smaller focal lengths such as 100

mm, combined with the light passing through the flat tunnel walls at a steeper angle, resulted in too much aspherical aberration at the final spot to obtain a meaningful signal. For this reason, a 200 mm focal length lens ahead of the tunnel and a 175 mm focal length lens following the tunnel were selected to achieve better spot quality at the sensor. The 175 mm focal length lens was placed on the translation apparatus such that the distance afterwards to the final focal point was around L = 900 mm, depending on the exact experiment, and the distance C can be measured as a percentage of L. In cases where C was a large enough fraction of L that the beam needed to be scaled down from 25.4 mm to 12.7 mm in order to reduce the spot size on the sensor while sacrificing beam size at the boundary layers, an iris was used between the collimator and the first lens. This iris cannot be placed after the tunnel because it would mask the deflections.

In order to obtain line-integral measurements from a conventional jitter probe for comparison, the two lenses and collimator were removed, and a 500 mm focal length lens was placed 500 mm ahead of the camera sensor, as schematically shown in Figure 5(b). The camera was placed at the focal point and the local beam jitter was measured by the conventional means.

III. Data Reduction

Beam displacement data was recorded using a Phantom v1611 high speed camera. The beam was converged to a small diameter spot on the camera from which the displacement could be directly extracted, taking care to avoid the attenuation at the exact focal point. The camera was placed at various distances way from the final lens in order to determine the effect of this distance on the spot quality and spectral quality. The beam displacement readings were divided by the distance C in order to find the beam angular displacement, otherwise referred to as the global beam jitter. The mean of the global beam jitter was removed, and the jitter power spectra were computed using a standard block averaging Fourier transform.

Obtaining reliable beam displacement data with the focused jitter probe requires an extra step of processing which is not required with the traditional Malley probe. All existing aero-optical measurement techniques using lasers typically rely on focusing the beam down to a small point to measure the overall centroid position of that point, and this act of focusing to a point tends to get rid of the effects of any intensity variations within the beam itself that do not affect the overall centroid motion. However, with larger spots, as is the case with the focused Malley probe or focused jitter probe, intensity variations inside the spot due to diffraction patterns from dust and other optical imperfections tend to affect the measurement, so additional processing must be done in order to determine the best way to capture the overall motion of the spot.

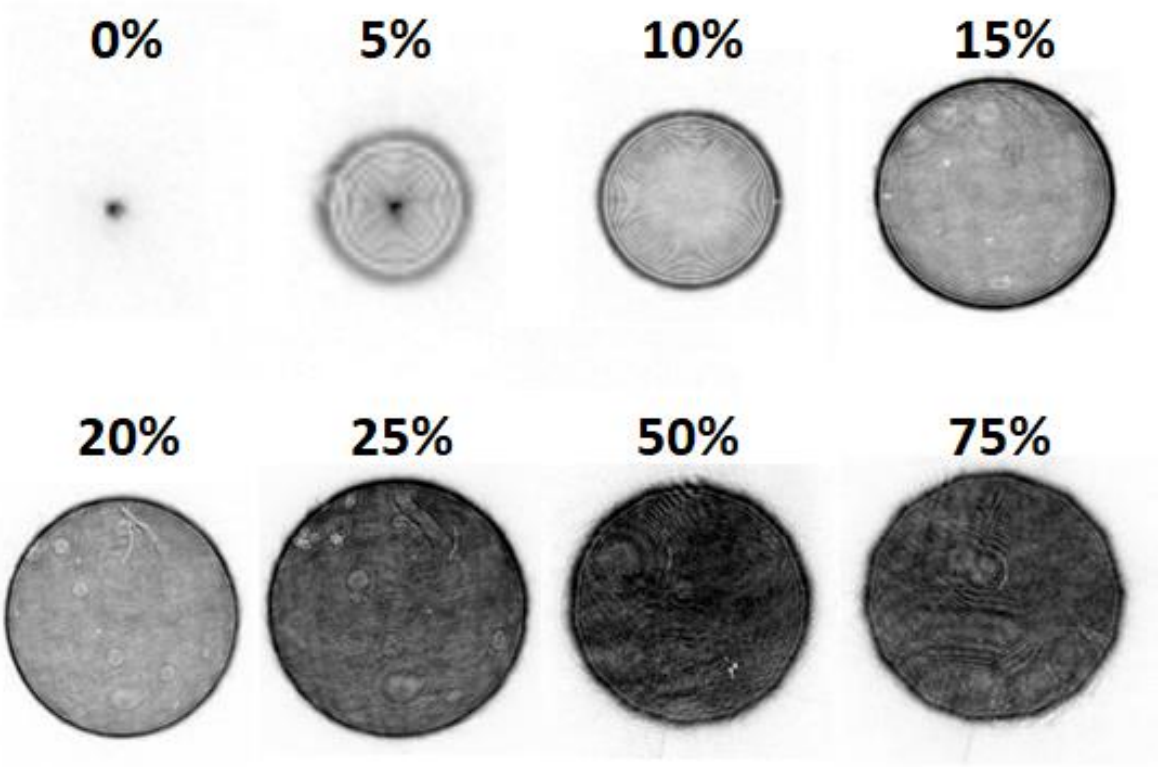

Figure 6: Variation in spot pattern while varying camera position C as percentage of L (Not to scale).

Figure 6 shows how the representative intensity pattern of the spot changes when the distance C is varied as a percentage of L, listed over each circle. The images are inverted, so darker areas correspond to greater light intensity. The 0% position is the focal point. When the camera is moved to the C/L=5% position, the spot pattern changes such that there is a pattern of rings around a bright central spot. At the 10% position, the central spot disappears while there are still prominent diffraction patterns visible inside a bright outer ring. At the 15% position, these diffraction patterns have mostly disappeared while there is still a bright outer ring. At this stage, there is lots of small-scale variation in the intensity pattern due to inevitable imperfections and dust particles on various mirrors, lenses, glass, and the camera sensor. While these were all cleaned to the best of our ability, having these random patterns is practically inevitable, so it is best to develop a postprocessing technique to handle them. While one could opt to have the diffraction patterns in the spots at the 5% position and the 10% position, these positions have smaller overall beam displacements due to the smaller distance from the focal point. At the 20% position, the diffraction patters within the bright outer ring disappear, and there are mainly intensity variations due to dust and imperfections within the outer ring. At the 25% position, the outer ring begins to fade and there may be points within the spot brighter than the outer ring. At the 50% and 75% positions, an iris was used so the spot would not be too large on the sensor. Because this results in a smaller aperture at the boundary layers, these last two configurations are not optimal.

The intensity-based method for determining the centroid of the beam, which is the standard for aero-optical measurements, consists of taking a weighted average centroid of the image,

calculated by the equation below, based on the intensity of each pixel at each instant in time. In this equation, p represents the pixel, x_p is the x-location, or y-location, depending on the direction chosen, of the pixel on the sensor, I_p is the intensity of the pixel, and N is the total number of pixels.

$$x_{centroid}(t) = \frac{\sum_{p=1}^{N} x_p I_p}{\sum_{p=1}^{N} I_p}$$

The thresholding method sets every pixel below a certain threshold value to zero intensity and every pixel above this intensity to one, or the maximum intensity when normalized, to help mitigate the effect of all the random intensity variations within the spot, shown in Figure 6, and to capture the overall motion of the spot instead. Judging by the intensity pattern, the threshold was chosen to be 40% intensity as a percentage of the maximum intensity. The beam centroid is calculated from these threshold intensities using the same equation above. Figure 7 below shows an original image from the high-speed camera (left), and the same image with the thresholding applied (right). Although a balance must be struck between masking faint areas within the spot and not capturing the faint areas outside the spot, the threshold still drastically reduces the noise by eliminating most of the intensity variations within the spot.

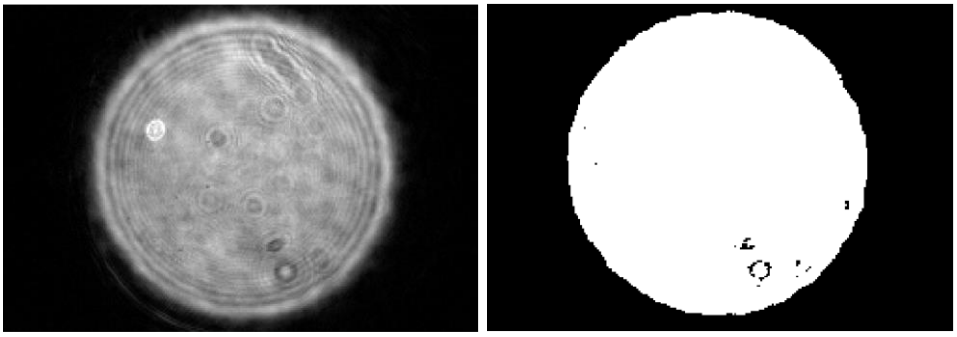

Figure 7: Spot without thresholding (left) and with thresholding (right) show masking of noise.

Once the centroid locations of the beam spot were known, the streamwise, or x-direction, global beam jitter was calculated by dividing the centroid positions by the distance C. Figure 8 shows global beam jitter resulting from the boundary layers of the Mach 0.4 flow through the empty tunnel for five different C/L locations, shown in the legend, using the intensity-based method, shown in Figure 8, left, and the thresholding method, shown in Figure 8, right. The frequency domain is plotted as a Strouhal number, given by the equation $St = \frac{fL_{Ref}}{U_\infty}$, where U_∞ is the free stream velocity, f is the frequency, and L_{Ref} is some reference length. In the case of the empty tunnel test, this length will be the boundary layer thickness δ = 15.6 mm, and in the case of taking measurements in the wake behind the cylinder, this length will be the cylinder diameter D = 3.175 mm.

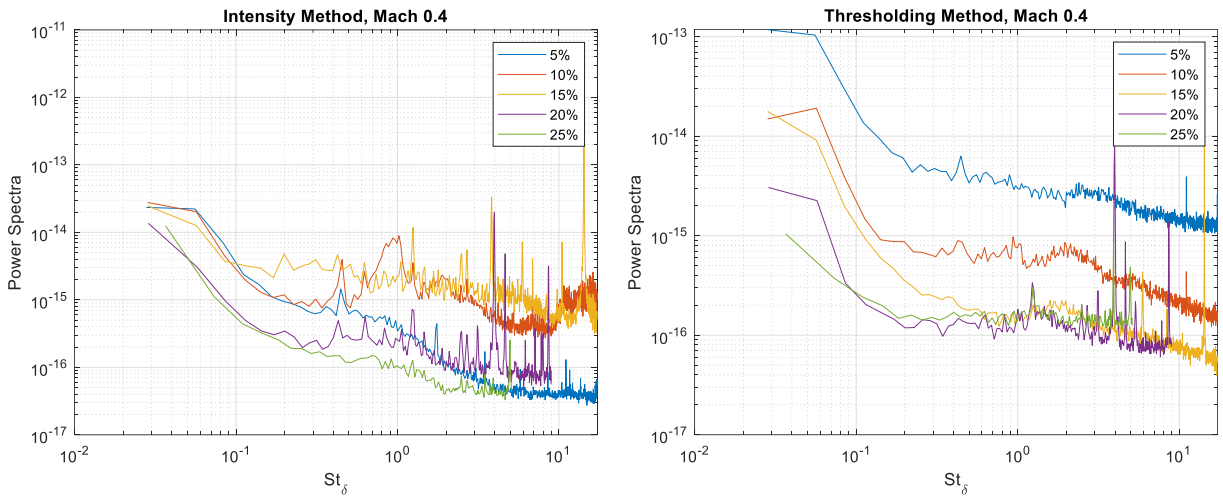

Figure 8: Beam jitter power spectra for empty tunnel using the intensity method (left) and the thresholding method (right) for various C/L ratios.

Without any corrupting effect, the spectra should collapse regardless of the centroiding method or C/L ratio. However, most of the random intensity variations within the spot due to diffraction patterns from dust and the like move rapidly relative to the spot, and do not correlate with the overall spot motion. For this reason, when the conventional intensity-based method is used, the spectra do not collapse for most C positions, as shown in Figure 8, left, indicating that the beam centroid is corrupted by all the random variations. The only exception might be the 5% location, due to the bright central spot and ring patterns overriding any other variations. However, because of the fact that smaller C positions result in a lower amplitude signal, this was not considered to be optimal for the focused jitter probe, although this could be an area of further study. The plot for the thresholding method, presented in Figure 8, right, on the other hand, shows a collapse between spectra for C/L positions larger than 10%. This shows that the thresholding method is able to capture the signal from the overall motion of the spot, while the intensity-based method is not.

To better illustrate noise-corrupting effects, Figure 9 illustrates the time series of the beam centroid in the streamwise direction using each method. As shown by the blue line, the noise levels for the intensity method is much higher due to all the intensity variations moving around within the spot itself. When these variations are removed with the thresholding method, they have less effect on the centroid, which better captures the overall motion of the spot, as shown by the red line, which has a much-reduced noise level. For all of these reasons, the thresholding algorithm will be applied for data analysis because it is a more robust and accurate method of measuring the spot displacement. An edge-based method, which computed the location of the bright outer ring present at around 15% to 20% and took the centroid, was also considered and tested, but this proved to be much more computationally intensive than the thresholding method while producing improvement over the intensity method, but to a lesser degree than the thresholding method, in the spectral results.

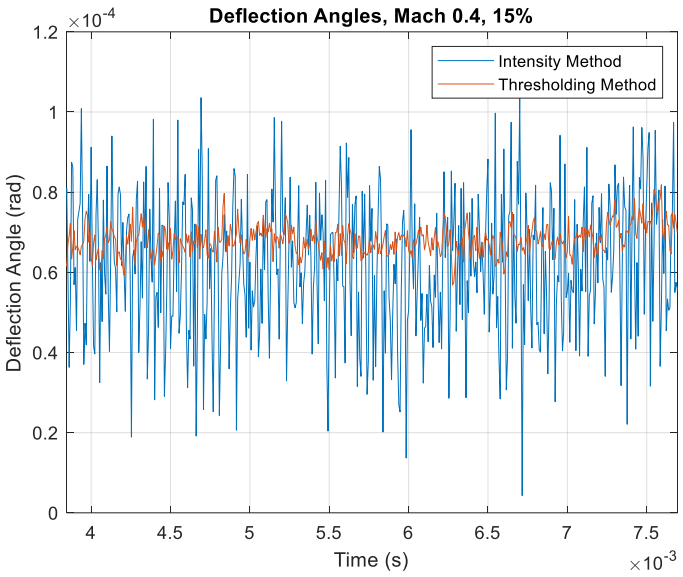

Figure 9: Representative time series of the global beam jitter computed using the intensity and thresholding methods shows reduced noise in thresholding method

IV. Results and Discussion

Figure 10 shows plots of the power spectra of the beam jitter in the streamwise direction at various spanwise locations of the focal point for the empty tunnel test on the left and for the flow downstream of the cylinder on the right. The distance C was selected to be 20% of the distance L for both of these cases. These plots show the spanwise locations of the focal point on the x-axis, the frequency on the y-axis, and the magnitude of the logarithm of the power spectra illustrated by color hue. The various spanwise locations were obtained by translating the focal point of the focused jitter probe using the translation apparatus. As usual, the low frequency noise is mainly due to mechanical vibrations. It can be seen in the plot for the empty tunnel in Figure 10, left, that for the mid-frequency range around 10 kHz, there is a dip in the magnitude near the center of the tunnel and a higher magnitude when the focal point is placed close to the boundary layer. This shows that the focused jitter probe behaved as intended, by primarily responding to the boundary-layer aero-optical distortions at the focal point when the point was placed close to either boundary layer, and by reducing the effects of the boundary layer when the focal point was moved away from them to the center of the tunnel.

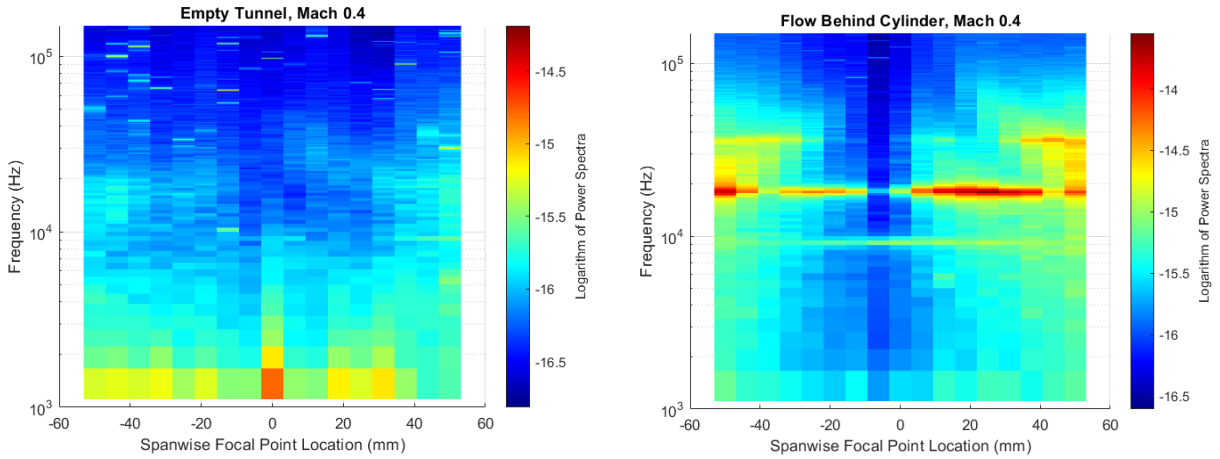

Figure 10: Power spectra of x-jitter at various spanwise locations for the empty tunnel (left) and the wake behind the cylinder (right) verify the functionality of the focused jitter probe

Using the 200 mm focal length lens ahead of the 100 mm wide tunnel with a 25.4 mm wide beam and a boundary layer thickness of 15.6 mm, the ratio of the beam aperture at the tunnel wall to the boundary layer thickness was $Ap/\delta = 0.4$. As illustrated by the corresponding turquoise line in Figure 3, left, this aperture should provide some beam jitter attenuation at frequencies above a few kHz where the spectra dips well below the spectra for the local jitter, shown by the blue line in Figure 3, left. Figure 10 shows that this is indeed the case, as the spectra for the focal point in the middle of the tunnel are attenuated at these frequencies, while the spectra with the focal point close to the boundary layer are not. However, in order to further prove the functionality of this technique, it should be used to measure a weaker signal in the center of the tunnel which cannot be discerned by conventional line-integral techniques due to the aero-optical effect of the boundary layers. This will demonstrate that the focused jitter probe can measure signals and discern local density information from the flow which the conventional jitter probe is unable to.

As mentioned before, this cylinder in the Mach 0.4 flow creates vortex shedding with a Strouhal number of 0.20 or a frequency of 9.5 kHz. Figure 11 shows wavefront measurements taken in the cylinder's wake, which illustrate the vortex shedding. The peak to peak distance between the visible aero-optical structures is around 7 mm, which corresponds to twice the vortex shedding frequency, or 19 kHz, when divided into the freestream speed, as expected. Indeed, the strongest signal should be twice the vortex shedding frequency because vortices are shedding off both sides of the cylinder and combining in the wake.

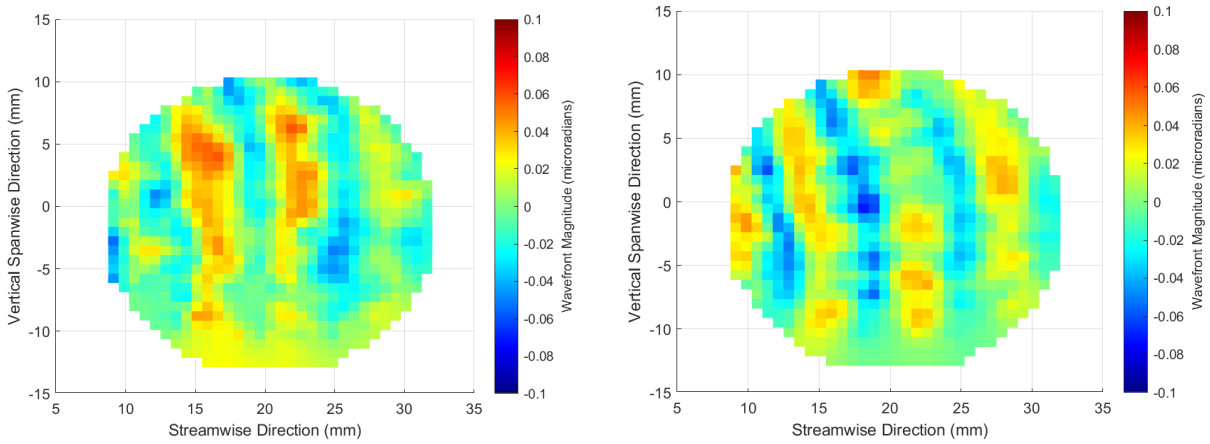

Figure 11: Representative wavefronts 2 cm downstream of cylinder showing spanwise aero-optical distortions indicative of vortex shedding.

As can be seen by Figure 10, right, for the case with the cylinder, there is a very strong spectrum at 19 kHz and a much fainter one right around 9.5 kHz, as expected. Also, the spectra are stronger with the focal point close to the tunnel walls than for the empty tunnel case. This might be attributed to the flow blockage created by the cylinder and its wake, which results in a velocity increase and stronger aero-optical signal from the boundary layers. The spectral peak at 19 kHz is clearly visible for all focal point locations, as this signal at this frequency is stronger than that from the boundary layers. On the other hand, the spectral peak at 9.5 kHz is not easily discernable when the focal point of the focused jitter probe was placed close the tunnel wall. However, this signal is clearly present when the focal point is placed at the center of the tunnel, as shown in Figure 10, right. This shows that the focused jitter probe functions as intended: when the focal point is located in the middle of the tunnel, it suppresses the jitter component from both boundary layers via the aperture averaging effect and is sensitive to the beam jitter primarily in the center of the tunnel.

To further study the effect of the focal point location on the resultant global beam jitter spectra, Figure 12 shows that for the empty tunnel test, the spectra measured with the focused jitter probe when the focal point is close to at either boundary layer agrees well with the local line-integral measurements from the conventional small-beam jitter probe, labelled as local jitter, 1mm beam in Figure 12. Deviations from this agreement are likely caused by some aliasing effects at higher frequencies due to the larger spot size requiring a larger pixel space, which required the data to be collected at a lower sampling frequency when compared with the conventional jitter probe. However, each technique has its own advantages and disadvantages, and this plot shows that even with an aperture to boundary layer thickness ratio of only $Ap/\delta = 0.4$, the aperture averaging effect was able to attenuate the aero-optical distortions from the boundary layers when the focal point was placed at the center of the tunnel test section away from any boundary layers. If custom made lenses are used to create larger convergent-divergent angles through the tunnel, the beam diameter at the boundary layers could be made larger to give a more significant attenuating effect. These sharper light angles are not possible with standard lenses because they create significant aspheric distortions and result in subpar spot quality. However, these

experiments with smaller angles and smaller apertures at the boundary layers still serve as a proof of concept for the focused jitter probe.

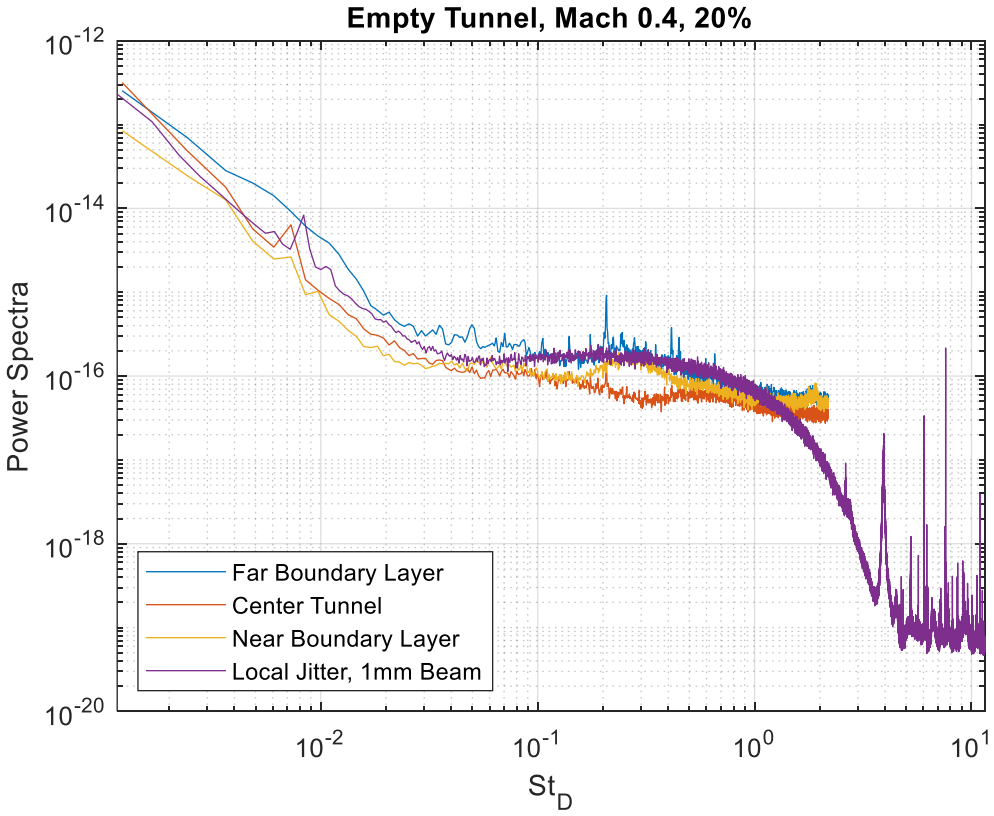

Figure 12: Focused jitter probe spectra for different focal point locations for the empty tunnel test demonstrate attenuation. Local jitter, measured using a conventional small beam jitter probe is also plotted for comparison.

Figure 13 shows that 2 cm downstream of the cylinder, the beam jitter spectra from the focused jitter probe with the focal point close to either boundary layer is very similar to the local line-integral spectrum from the conventional jiter probe, labelled as local jitter, 1mm beam in Figure 13. The camera is placed 20% of the final distance away from the final focal point. The empty-tunnel local jitter spectrum is shown for comparison. There is a large spike at twice the shedding frequency at $St_D = 0.4$ present in all spectra for the case with the cylinder present. A smaller spike at the shedding frequency of $St_D = 0.2$, which is hardly visible in the baseline spectrum, is somewhat visible in the spectra when the focal point is close to either boundary layer, and is very pronounced when the focal point is placed inside the cylinder's wake. This again verifies that the focused jitter probe ulilizes aperture averaging to atenuate jitter signals in the regions of the flow away form the focal point and makes jitter signals at the location of the focal point more visible. This attenuation due to aperture averaging is clearly visible between around 1kHz to 80kHz, or between Strouhal numbers of around 0.03 to 2.

As a final note, all global beam jitter spectra measured by the focused jitter probe show energy build up at the high end of the spectra. This was attributed to the spectral aliasing, since in

order to accommodate the larger spot size, the sampling frequency on the high-speed camera had to be reduced to 190 kHz.

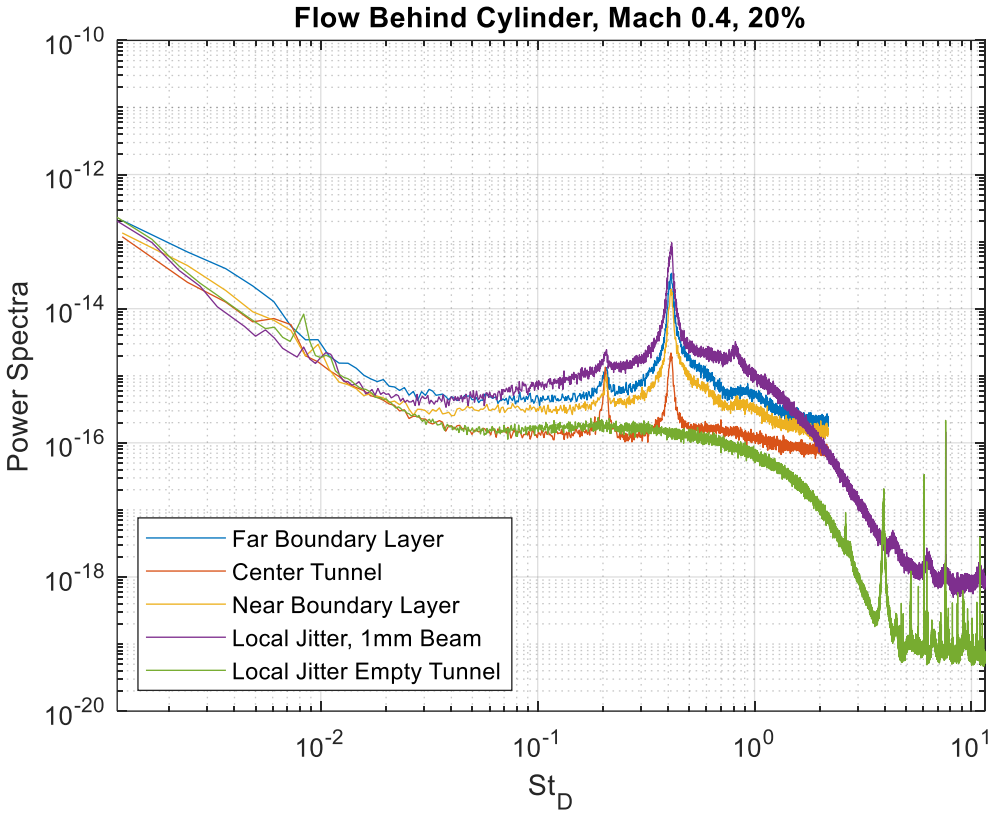

Figure 13: Focused jitter probe spectra for different focal point locations for the flow in the cylinder's wake demonstrate attenuation. Local jitter, measured using a conventional small beam is also plotted for comparison.

V. Conclusions and Future Work

A non-intrusive point aero-optical jitter measurement technique, termed the focused jitter probe, was developed. This probe can attenuate the signals from the boundary layers present on the tunnel walls in order to discern the density-related aero-optical fluctuations near the focal point. By comparison, the conventional jitter probe, which is a line-integral measurement technique, measures the overall jitter, and cannot discern where aero-optical distortions occur along the beam. By using an expanded beam and lenses to create a converging-diverging beam inside the tunnel test section, a focal point can be placed in the center of the tunnel. This convergent-divergent arrangement also creates the larger beam diameters at the tunnel walls, where the boundary layers are present. The large beam diameter suppresses the corrupting aero-optical effects of the boundary layers due to the aperture averaging effect. Thus, the global beam jitter is primarily caused by the local aero-optical distortions in the vicinity of the focal point. To measure the global beam jitter, the laser beam was focused to a point outside of the tunnel, and different sensor placements relative to that focal point were tested to study the sensitivity of the measurements to the sensor placement.

Due to inevitable intensity variations within the beam spot due to various optical contaminations, a thresholding algorithm was proposed and applied to correctly measure the time-dependent global beam jitter.

The focused jitter probe was tested at a subsonic speed of Mach 0.4 with two flow configurations. The first configuration, labelled the empty tunnel test, was with only turbulent boundary layers present at the tunnel walls. For another configuration, labelled the cylinder flow test, a small cylinder was placed in the spanwise direction perpendicular to the beam in the middle of the test section to create strong localized aero-optical distortions from vortex shedding. For the empty tunnel test, when the focal point was placed close to the boundary layers, the global beam jitter spectra resembled those measured using the conventional jitter probe. When the focal point was placed in the center of the tunnel, spectral attenuation was clearly visible. For the cylinder flow test, a spectral spike was clearly visible at twice the vortex frequency in all spectra regardless of the location of the focal point. However, the weaker spike at the vortex shedding frequency was more pronounced with the focal point placed at the center of the tunnel, demonstrating the suppression of the boundary layer effects away from the focal point. These experiments demonstrate that the focused jitter probe can be used to infer local information about the aero-optical flow which would otherwise be combined with the corrupting effects from the boundary layers if any conventional line-integral technique were used.

The concept of a focused jitter probe can be extended to a focused Malley probe, with two convergent-divergent beams having focal points in the tunnel with a small separation apart in the streamwise direction. The time-dependent beam jitter from both beams can be used to cross-correlate the signals and to obtain a local velocity measurement. In comparison, the line-integral velocity measurement of the traditional Malley probe is a weighed integral of all velocities along the beam, and might be potentially corrupted by the strong aero-optical signals from the boundary layers at the tunnel walls, especially at very high velocities. In future studies, the focused Malley probe will be designed, and the beams' cross-correlations will be experimentally measured in order to extract speed measurements and compare with theoretical values for selected canonical flows. These measurements will also be compared against those from a traditional Malley probe in order to quantify the focusing ability and attenuating effects of this novel measurement technique. Also, the accuracy of the measurements for the focused jitter probe will be further studied using the simulated phase screens approach.

Acknowledgements

This work is supported by the Air Force Research Laboratory, Cooperative Agreement number FA9451-18-2-0088. The U.S. Government is authorized to reproduce and distribute reprints for governmental purposes notwithstanding any copyright notation thereon.

References

[1] S. Gordeyev, E.J. Jumper, "Physics and Measurement of Aero-Optical Effects: Past and Present," Annual Review of Fluid Mechanics, **49**, pp. 419–441, 2017

[2] S. Gordeyev, A. E. Smith, J.A. Cress and E.J. Jumper, "Experimental studies of aero-optical properties of subsonic turbulent boundary layers," *Journal of Fluid Mechanics*, **740**, pp. 214-253, 2014.

[3] S. Gordeyev, T. Hayden and E. Jumper, "Aero-Optical and Flow Measurements Over a Flat-Windowed Turret", *AIAA Journal*, **45**(*2*), pp. 347-357, 2007.

[4] S. Gordeyev, J.A. Cress, A Smith and E.J. Jumper, " Aero-optical measurements in a subsonic, turbulent boundary layer with non-adiabatic walls", Physics of Fluids, 27, 045110, 2015.

[5] Malley M, Sutton GW, Kincheloe N. 1992. Beam-jitter measurements of turbulent aero optical path differences. Appl. Opt. 31:4440–43.

[6] Fitzgerald, E., and Jumper, E. (2004). The optical distortion mechanism in a nearly incompressible free shear layer. Journal of Fluid Mechanics, 512, 153-189.

[7] N. De Lucca, S. Gordeyev, and E. Jumper, "The Study of Aero-Optical and Mechanical Jitter for Flat-Windowed Turrets", AIAA Paper, 2012-0623.

[8] B. Vukasinovic, A. Glezer, S. Gordeyev, E. Jumper and V. Kibens, "Fluidic Control of a Turret Wake: Aerodynamic and Aero-Optical Effects", AIAA Journal, Vol. 48,No, 8, pp. 1686-1699, 2010.

[9] J. Sontag and S. Gordeyev, "Non-intrusive Velocity and Density Measurements in Subsonic Turbulent Boundary Layer ", AIAA Paper 2015-3247, 2015.

[10] M.R. Kemnetz and S. Gordeyev, "Multiple aperture approach to wavefront prediction for adaptive-optic applications," AIAA Paper 2017-1344, 2017.

[11] L. Butler and S. Gordeyev, "Effect of Varying Beam Diameter on Global Jitter of Laser Beam Passing Through Turbulent Flows", AIAA Paper 2019-3385, 2019.

[12] B. E. Schmidt and J. E. Shepherd. "Analysis of Focused Laser Differential Interferometry." Applied Optics, 2015.

[13] Matthew R. Fulghum. "Turbulence Measurements in High-Speed Wind Tunnels Using Focusing Laser Differential Interferometry." Pennsylvania State University, 2014.

[14] N. J. Parziale, J. E. Shepherd, and H. G. Hornung. "Observations of Hypervelocity Boundary-Layer Instability." Journal of Fluid Mechanics, Cambridge University Press, 2015.

[15] N. J. Parziale, J. E. Shepherd, and H. G. Hornung. "Differential Interferometric Measurement of Instability in a Hypervelocity Boundary Layer." AIAA Journal 51:3, 2013.

[16] Potts, Andrew E., Potts, Douglas A., Marcollo, Hayden, and Jayasinghe, Kanishka, "Strouhal Number for VIV Excitation of Long Slender Structures", ASME, No. OMAE2018-77433, V005T04A073, 2018.